STATISTICS OF SOLAR EUV JETS

© 2025 I.P. Loboda*, S.A. Bogachev, A.S. Kirichenko, A.A. Reva, A.S. Ulyanov
Space Research Institute, Moscow, Russia
**e-mail: ivan.loboda@cosmos.ru*

Received March 04, 2024
Revised August 12, 2024
Accepted for publication August 12, 2024

Collimated ejecta of matter, otherwise known as jets, are observed in large numbers in the chromosphere and lower corona of the Sun, and are of great interest in relation to their possible role for the transport of matter and energy in the solar atmosphere. These jets are subdivided into several groups characterized by different formation mechanisms and substantial variation of their characteristics. In order to distinguish separate groups of jets and identify them with respective formation mechanisms, we performed a statistical study of the full ensemble of solar extreme ultraviolet (EUV) jets using observations from the Solar Dynamics Observatory (SDO) in the 171, 193, and 304 Å channels. We identified a total of 212 such events, of which 26% were classified as linear jets, probably generated by magnetoacoustic shocks, and 30% as helical jets, representing small-scale filament eruptions. We found that these two groups differ significantly in their major dynamic characteristics (maximum height, initial velocity, and lifetime), as well as in their widths that are closely related to the underlying magnetic field structure, while helical jets were also shown to be much more frequently associated with the presence of hot coronal component. At the same time, we found a third class of jets with intermediate characteristics and unknown formation mechanism, requiring further study.

DOI: 10.31857/S00234206250104e4

INTRODUCTION

In the chromosphere and lower corona of the Sun, a large number of relatively small-scale transient phenomena are observed, known under the general name of solar jets, which are fast jet-like directed flows of matter rising above the photosphere [1]. Accordingly, solar jets traditionally attract significant research interest in terms of their possible role in mass and energy transfer processes in the solar atmosphere, but many questions still remain regarding their detailed contribution to these processes, as well as their own formation mechanism [2, 3].

Solar jets are observed everywhere, both in active regions and in quiet Sun regions and coronal holes, varying significantly in scale, structure, and dynamics. At the same time, their study is largely complicated by the fact that solar jets possess significant diversity, both in their sizes and dynamic characteristics (Fig. 1), as well as in temperature and, accordingly, are observed in different spectral ranges. As a result, it becomes difficult to identify structures observed in multiple spectral channels using various instruments [4, 5]. Furthermore, the definition of solar jets and their individual subtypes remains quite broad and is primarily related to morphological structures visible in solar images without reference to specific physical mechanisms. Thus, this definition potentially encompasses a wide class of processes in the solar atmosphere, which probably have different physical nature and formation mechanism.

Fig. 1. Differences between the main types of solar jets by rise height and lifetime

Among the main groups of solar jets, the most small-scale and at the same time most numerous variety are chromospheric spicules, which have characteristic longitudinal dimensions of 4–18 thousand. km, transverse - from 300 to 2500 km, and lifetime in the range of 2-12 min. The spicule material is predominantly chromospheric in its characteristics, has a temperature of 7000 to 16000 K and density in the range of $4 \cdot 10^{10}$-10^{12} cm^{-3}. Their movement speed is relatively small and amounts to 20-60 km/s [6]. The probable mechanism of spicule formation is considered to be the ejection of chromospheric material by shock magnetoacoustic waves formed during the transition of photospheric sound oscillations through the sharp (in terms of density gradient) boundary between the chromosphere and corona [7, 8].

At the opposite end of the spectrum are significantly larger coronal jets, observed mainly in X-ray images of the Sun, which is due to the high temperature of their material from $4 \cdot 10^{5}$ to $2.8 \cdot 10^{7}$ K, while the density of coronal jets is substantially lower and is about $7 \cdot 10^{8}$-$5 \cdot 10^{10}$ cm^{-3}. The characteristic lifetime of coronal jets is in the range from 10 min to 7 h and more, speed - from 90 to 1100 km/s, rise height is about 20-500 thousand km, and width - about 6-10 thousand km [9]. Relatively recently, a special subclass of coronal jets was identified - the so-called blowout jets, which are characterized by spiral movement of material around the central axis of the jet, generated by the eruption of a small-scale filament (minifilament) as a result of reconnection of the twisted magnetic tube that held it with the surrounding, predominantly unipolar, magnetic field structure [10]. These types of jets often have a significantly colder component that is well visible in the spectral lines of vacuum ultraviolet (VUV) [11].

An intermediate position between chromospheric spicules and coronal jets, both in terms of spatial and temporal scale, as well as characteristic plasma temperature, is occupied by jets observed in the EUV range. Historically, such jets are called macrospicules because in the first EUV images of the sun obtained by the space observatory *Skylab* which had relatively low angular resolution, they were identified as chromospheric spicules, having, however, a significantly larger size [12]. Thus, this term primarily reflects the visual similarity of EUV jets to spicules without reference to a specific structure and the probable formation mechanism, which remains not reliably established. Often, any jets observed in EUV lines are called macrospicules, regardless of their morphological structure, which further blurs the meaning of this term and complicates the identification of jets.

Also, there are reasons to believe that at least some of the smallest EUV jets actually represent the hot component of the largest chromospheric spicules [13, 5]. Previously, the authors identified a subset of EUV jets representing narrow, collimated matter ejections, which in the context of this work are conveniently called linear. A characteristic feature of the dynamics of such jets is parabolic (i.e., having a quadratic dependence on time) profiles of their apex movement, which are not, however, ballistic and apparently arise as a result of matter acceleration in accordance with the linear velocity profile of the ascending magnetoacoustic shock wave, similar to the formation mechanism of smaller-scale chromospheric spicules [14, 15]. Accordingly, it can be said that this variety of EUV jets most deserves the name of macrospicules.

EUV jets, as well as solar jets in general, have a wide range of observed characteristics. In particular, as noted above, the largest of them are often identified with the cold components of X-ray jet-ejections [11]. Accordingly, at least two significantly different mechanisms for the formation of jets observed in the EUV range can be distinguished: one is associated with the eruption of minifilaments, accompanied by a significant restructuring of the original magnetic field

structure, while the other is formed as a result of a purely hydrodynamic process in which the role of the magnetic field remains predominantly passive. This raises the question of investigating the boundary between these two groups of jets and their mutual relationship—whether these groups can be unambiguously separated by observable characteristics, and whether such a separation can describe the entire set of jets observed in the EUV.

To answer this question, a large-scale statistical study is needed, in which all groups of jets observed in the EUV range will be equally well represented. The literature typically presents only individual observations of such jets, often incidental to observations of other solar activity phenomena, and the few attempts at statistical studies of this variety of solar jets have in all cases been significantly limited by the criteria for selecting events to simplify their identification and measurement of characteristics [16, 17]. The present study aims to examine the entire population of solar jets observed in the EUV range, with the goal of unified registration and measurement of the characteristics of events observed beyond the limb and identification of all existing groups of jets to establish their formation mechanisms and mutual relationships.

DATA AND METHODS

The best opportunity for such statistical studies is currently provided by the AIA telescope complex of the *Solar Dynamics Observatory* (*SDO*), which conducts regular observations of the disk and lower corona of the Sun in 7 narrow spectral channels of the EUV range [18]. A distinctive feature of these observations is their high spatial (1.2 arc sec, or about 870 km) and temporal (from 6 s) resolution with a continuously observed full solar disk in a field of view of 41×41 arc min.

For reliable and unambiguous identification of jets, it is most convenient to use the off-limb region of images. In this study, the 304 Å channel is used to identify individual events, which is dominated by the transition layer line of He II 304 Å, highlighting the thin boundary between, typically, cooler matter inside the jet and coronal matter outside. It is important to note that beyond the limb, the coronal line of Si XI ion also contributes significantly to this channel, which complicates the identification of faint structures behind the limb. To eliminate this, a semi-empirical model proposed in the work [19] was used.

To study the "hot" (coronal) and "cold" (chromospheric) components of jets, AIA observations in 171 and 193 Å channels were additionally used. In these channels, both hot jet material can be observed in emission, if its differential emission measure (DEM) becomes comparable to the DEM of the quiet corona along the line of sight, and cold, chromospheric material, containing a significant amount of neutral hydrogen, visible in absorption due to its photoionization, as well as due to the absence of coronal material in the corresponding region of space. Accordingly, such observations can be interpreted either as a sign of heating of part of the jet material due to small-scale magnetic field line reconnection, or as the presence of dense cold material concentration in the jet, usually - an ejected minifilament. In addition, independent identification of events was carried out in the 171 and 193 Å channels, which, however, did not show the presence of jets not registered in the 304 Å channel. An example of simultaneous observation of an EUV-range jet in the specified spectral channels is shown in Fig. 2.

Fig. 2. Example of observations of an ejection jet, formed by a minifilament eruption, in channels 304 Å (a), 171 Å (b) and 193 Å (c) *SDO/AIA* . In channels 171 and 193 Å (b, c) the movement of cold minifilament material is visible at the initial stage of jet movement, while in the 193 Å channel (c) the ejection of hot coronal material is simultaneously visible.

For the study, 4 three-hour intervals from 9:00 to 12:00 UT were selected, each on May 14 from 2010 to 2014 , in which the AIA observation time step in all spectral channels used was uniform and equal to 12 s. Despite the fact that *SDO* continues to operate until the present moment, later observation periods were not considered due to significant degradation of the 304 Å channel [20], which significantly reduced the efficiency and, most importantly, the uniformity of recording jets beyond the limb. In the corresponding images, an over-the-limb region was identified, located from 10 thousand km below the limb to 80 thousand km above it, sufficient for observing the bases and full length of EUV jets. Areas occupied by large-scale activity phenomena - active regions and prominences - were excluded. For convenience of data processing, a polar transformation of the specified area was performed, after which three-dimensional arrays (data cubes) were compiled from individual images $D[\varphi,h,t]=\frac{1}{\Delta t}I_t\left[(R+h)\cos\varphi-x_0,(R+h)\sin\varphi-y_0\right]$, where $I_t[x, y]$ — original image obtained at time t; Δt — exposure time; x_0 and y_0 — coordinates of the Sun's center in the image; R and h — radius of the Sun and height above the limb; φ — polar angle measured from the Sun's north pole; meanwhile, the interpolation step for φ and h was selected in accordance with the angular resolution of AIA. Subsequent processing of the observational data prepared in this way was carried out in a semi-automatic mode.

For reliable registration of all observed events beyond the limb, synoptic maps at various heights h_s were used, representing slices $S[\varphi, t] = D[\varphi, h_s, t]$. To scan by height, as well as identify and catalog individual events on such maps, a graphical interface was developed, allowing processing of large amounts of observational data in a short time, and, accordingly, collecting a statistically significant sample of events. After identifying with such maps the area $C = D[\varphi_1:\varphi_2, h, t_1:t_2]$, isolating each event by time and position on the limb, a map of the greatest intensities over time $M[\varphi,h]=\max_t C[\varphi,h,t]$ was constructed. This allowed accurately identifying the jet axis and the magnetic flux tube containing its matter throughout the observed lifetime, even in the case of intense internal motions of the jet matter during its development. Thus, the position of the jet axis and its inclination to the normal were determined, as well as the width of the jet itself; the position of the jet on the limb was registered as the point of intersection of its axis with the visible limb of the Sun.

After that, to study the longitudinal dynamics of the jet matter movement, space-time maps were constructed, obtained by averaging the observed intensity over horizontal layers within the magnetic flux tube containing the jet matter: $T[h,t]=\frac{1}{2\Delta\varphi}\sum_{\varphi_a-\Delta\varphi}^{\varphi_a+\Delta\varphi}C[\varphi,h,t]$, where $\varphi_a = \varphi_a(h)$ — is the position of the jet axis; $2\Delta\varphi$ — is its width. Due to the relatively weak intensity of jet radiation compared to the quiet corona radiation, it was necessary to additionally increase the contrast of observations. For this purpose, before averaging the intensity, the median signal over time in the corresponding spectral channel, calculated at each point of the corona (φ, h) for the full observation period, was subtracted. Using such space-time maps, other main characteristics of the jet were measured — the height of its rise, the initial velocity of movement, and the observed lifetime, characterizing the overall dynamics of the jet matter movement along its axis.

Since this study was aimed at statistical, as uniform as possible examination of the entire ensemble of EUV jets, rather than a detailed study of individual phenomena, only the above-

mentioned main parameters characterizing the spatial scale and dynamics of jets were recorded. For identification of observed events with the main known formation mechanisms, the presence of parabolic (over time) profiles of the jet apex movement with a generally collimated nature of its matter movement was separately recorded as an indicator of the acceleration mechanism by shock waves, and the presence of axial, spiral-like rotation of the jet simultaneously with mini-filament eruption at its base. Accordingly, such jets were classified as eruptive jets. Due to the weak observed absorption and emission of jets in "hot" channels 171 and 193 Å, their dynamics in these channels was not studied in detail; only the presence of a significant reduction or enhancement of emission in these channels compared to the background noise within the magnetic flux tube of the jet was recorded.

RESULTS

During the selected observation period, 212 separate events were identified, 65% of which were observed in quiet sun regions and 35% in coronal holes. The latitudinal distribution has a pronounced peak near the poles (Fig. 3a) due to the higher concentration of jets in coronal holes, which during the studied period were predominantly polar. Thus, despite the smaller absolute number of recorded events, the rate of appearance of jets of all possible classes is significantly higher in coronal holes, which compensates for the relatively small area of the latter compared to quiet Sun regions. The inclination of the axis of all registered jets was, as a rule, within ±40°, which indicates their connection with a predominantly vertical, unipolar configuration of the magnetic field near photospheric concentrations of magnetic flux. In addition, the obtained data confirmed the existence of a significant difference in the rise height of jets observed in coronal holes and in the quiet sun (Fig. 4b), similar to the previously discovered dependence for spicules and macrospicules [8, 21]. This pattern is the same for all types of registered events, which indicates an equal role in the development of various classes of EUV jets of predominantly unipolar magnetic field configuration and lower hydrodynamic resistance of the surrounding plasma, characteristic of coronal holes.

Fig. 3. Distribution of the main measured characteristics of solar EUV jets. Jets registered in quiet sun regions and in coronal holes (a, b), linear and spiral jets (c-g), and jets that had noticeable absorption or emission in channels 171 and 193 Å (h-j) are shown separately.

Fig. 4. The strongest correlations of measured jet characteristics. The color indicates the year of observation. Dashed lines show linear approximations along with the corresponding correlation coefficient values.

Of all observed events, 56 jets (26% of the total) were identified as linear and 63 (30%) as spiral, with only 56 of them (26% of the total) associated with an observed ejection of a small-scale minifilament at their base, which allows additionally identifying such events as blowout jets. When comparing the characteristics of the two main populations of EUV jets, also shown in Table 1, linear jets have a noticeably lower average rise height — 19 versus 29 thousand km (Fig. 4c), magnetic tube width — 4 versus 14 thousand km (Fig. 4d), and significantly higher ratio of jet height to width (Fig. 4e), i.e., the differences mentioned above are not a consequence of just a proportional increase in jet scale. Thus, linear jets are not only less extensive but also much narrower, more collimated structures, which generally corresponds to the purely hydrodynamic

nature of material movement in the magnetic tube, which can be arbitrarily narrow in the general case, while for blowout jets, the width of the magnetic tube is fundamentally limited from below by the size of the initial structure of the ejected minifilament. The latter circumstance is also reflected in the obtained distributions: the smallest width of registered spiral jets is 8 thousand. km, which is significantly larger than not only the minimum but also the average width of linear jets.

Table 1. Main measured characteristics of EUV-range jets, their linear and spiral subgroups (the most characteristic values are indicated).

Characteristic	All jets	Linear jets	Spiral jets
Rise height, thousand km	22.7	18.9	28.6
Width, thousand km	7.2	4.0	13.9
Height/width ratio	2.6	3.0	1.8
Initial velocity, km/s	58.3	50.4	80.0
Lifetime, min.	10.8	8.4	16.5
Percentage of total number, %	—	26.4	29.7
Visibility in absorption, %	57.1	60.7	71.4
Visibility in emission, %	28.3	10.7	41.3

When comparing dynamic characteristics, spiral jets also have significantly higher characteristic values — their average initial velocity is about 80 km/s versus 50 km/s for linear jets (Fig. 3e), which, in turn, results in a noticeably longer lifetime of such jets — 16.5 versus 8.5 min. (Fig. 3g); which generally characterizes them as larger and more energetic activity phenomena. It can be noted that all the obtained distributions for spiral jets are significantly wider than for linear ones, which indicates their greater variability, apparently due to a more complex formation mechanism determined by a greater number of external factors and initial conditions. An important circumstance is that the remaining 45% of the observed jets could not be unambiguously assigned to either of the main classes mentioned above based on their dynamic and morphological characteristics, while in terms of their main parameters characterizing their scale and overall energetics, such jets occupy an intermediate position between these classes.

When examining the signal in the "hot" AIA channels, it was found that 61% of linear jets were visible in absorption in one of these channels, and only 11% were visible in emission relative to the background of the undisturbed corona. In contrast, among spiral jets, 71% were visible in emission, and 41% in absorption, indicating a somewhat higher total line-of-sight density of chromospheric material in such jets, as well as significantly more intense heating of the material to coronal temperatures. The most likely source of such heating could be the process of small-scale magnetic reconnection, apparently involved in the formation of spiral jets. Overall, in the 171 Å channel, 60 jets (28% of the total) were visible in emission, and 98 jets (46%) in absorption, while in the 193 Å channel, corresponding to a higher temperature of the emitting plasma, 24 jets (11%) were visible in emission, and 115 (54%) in absorption. This may indicate that despite the probable heating of material in a significant portion of the observed jets, its intensity may be sufficient to reach coronal temperatures only in the largest, most energetic events, which are more likely to belong to the class of spiral jets. It was also shown that, in general, jets visible in emission (and

thus associated with heating of a substantial fraction of their material to coronal temperatures) have only slightly greater rise heights compared to jets visible in absorption (respectively, representing predominantly cold material flows; Fig. 3h). The latter, however, are characterized by significantly lower velocities (Fig. 3i) and lifetimes (Fig. 3k), which confirms the connection between the overall dynamics and energetics of the jet with the intensity of energy release processes and plasma heating within it.

In addition to distributions, the interrelationship of the measured characteristics was also investigated, showing the presence of significant correlations between a number of basic parameters for all types of jets. First of all, we can note the pronounced interdependence of the rise height, initial velocity, and lifetime of jets (Fig. 4a-c), which could be explained by similarity effects when changing the scale of observed events. In addition, however, a strong correlation was found between the height of rise and lifetime of jets with their width (fig. 4d,e), and a somewhat less pronounced correlation between width and initial velocity of jets (fig. 4e). The presence of such correlations once again emphasizes the role of the initial magnetic structure in the predominant mechanism of formation and overall energetics of the jet. Furthermore, no significant variation in the observed characteristics of jets was recorded throughout the solar cycle, both in terms of the distribution of these values and in terms of their correlations.

Finally, when considering the subgroup of spiral jets, which from a physical mechanism perspective represent mini-filament eruptions, it is interesting to compare them with the family of larger filaments or prominences, observed in large numbers almost everywhere on the disk or beyond the limb, respectively. For this purpose, an array of observations was used, obtained from EUV telescopes *TESIS* of the space observatory *CORONAS-Photon* in the 304 Å channel and including about 400 predominantly small-scale quiet and quiet-eruptive prominences [22]. Based on these data, a relationship was found between the lifetime of prominences and a number of other characteristics reflecting their scale, such as the apparent projection area, as well as the estimates of volume, mass, and gravitational energy of prominences obtained in the work. The observed spectrum of these characteristics indicated an increase in the number of prominences with decreasing corresponding scale, which suggested the likely presence of a large number of smaller-scale structures when extrapolated to the region of smaller values.

Thus, one can expect that a similar pattern should be observed for the subgroup of spiral jets observed in this work. To estimate the mass-energy characteristics of jet-ejections, the same evaluation model was used as in [22], while for the possibility of comparing results, a mutual calibration of intensity in the 304 Å channels of telescopes *AIA* and *TESIS* was conducted, separately for each observation period considered in this work, to account for the significant degradation over time of the 304 Å channel of the *AIA* complex. Despite the fact that the number of reliably registered jet-ejections was insufficient to form a statistically significant sample, they do indeed exhibit a similar relationship between the scale of the event and its lifetime, albeit with a very low correlation coefficient (Fig. 5a). Moreover, the registered jet-ejections accurately continue the dependency observed for larger prominences. It is worth noting that such a direct comparison may not be entirely correct, since in the present work only the ejection material is observed, not the mini-filament at its base, and only the time of visible movement behind the limb of the resulting jet is recorded. Probably, such a good correspondence can be explained by similarity effects, as well as by the fact that for smaller-scale structures, the duration of the ejection may be comparable to the lifetime of the mini-filament itself.

Fig. 5. The interdependence of lifetime and scale, expressed by average gravitational energy, for prominences and jet-ejections (a), as well as for different groups of jets (b). Dashed lines show linear approximations: red — for jet-ejections, black — for prominences (a) and all types of EUV jets (b).

At the same time, if we consider the "lifetime – scale" relationship for the entire set of studied jets, a similar pattern is discovered, which, however, has a significantly different power exponent from the one described above (Fig. 5b). At the same time, jets identified as linear occupy the region of the smallest scales, while spiral jet-ejections, on the contrary, have the highest values of lifetime and energy, while a significant part of the registered jets that do not belong to either of the main groups represents a gradual transition from one group to another. This once again indicates the presence of an important, transitional variety of EUV-range jets with a still unclear formation mechanism, without detailed study of which, primarily from the perspective of understanding their physical nature, a complete description of the entire set of solar jets is impossible.

CONCLUSION

In this work, a statistical study of the entire population of solar jets observed in the EUV range was conducted in order to identify different groups that differ in their formation mechanism. It is shown that linear jets, for which the most probable mechanism is the acceleration of matter by a shock wave, and spiral jets, which are mini-filament eruptions, differ significantly in their main spatial and dynamic characteristics, primarily in width, which indicates the importance of the initial topology of the magnetic structure in the formation of these jet groups. At the same time, the presence of an intermediate group of jets is shown - transitional in its characteristics between linear and spiral, for which the probable formation mechanism remains undetermined. Thus, further, more detailed study of this subset of EUV-range jets is required in order to establish their physical nature and mutual relationship with other types of solar jets.

FUNDING

This work was supported by a grant from the Russian Science Foundation (project No. 21-72-10157).

CONFLICT OF INTERESTS

The authors declare that they have no conflict of interest.

REFERENCES

1. *Shen Y.* Observation and modelling of solar jets // Proc. the Royal Society A. 2021. V. 477. Iss. 2246. Art.ID 20200217. DOI: 10.1098/rspa.2020.0217.
2. *De Pontieu B., McIntosh S.W., Carlsson M. et al.* The origins of hot plasma in the solar corona // Science. 2011. V. 331. Iss. 6013. P. 55–58. DOI: 10.1126/science.1197738.
3. *Loboda I.P., Bogachev S.A.* Plasma dynamics in solar macrospicules from high-cadence extreme-UV observations // Astron. Astrophys. 2017. V. 597. Iss A78.0. P. 1963–1980. DOI: 10.1051/0004-6361/201527559.
4. *Wang H.* Comparison of Hα and He II λ304 Macrospicules // The Astrophysical J. 1998. V. 509. Iss. 1. Art.ID 461. DOI: 10.1086/306497.

5. *Skogsrud H., Rouppe van der Voort L., De Pontieu B. et al.* On the temporal evolution of spicules observed with IRIS, SDO, and Hinode // The Astrophysical J. 2015. V. 806. Iss. 2. Art.ID 170. DOI: 10.1088/0004-637X/806/2/170.

6. *Sterling A.C.* Solar spicules: a review of recent models and targets for future observations // Solar Physics. 2000. V. 196. P. 79–111. DOI: 10.1023/A:1005213923962.

7. *De Pontieu B., McIntosh S., Hansteen V.H. et al.* A tale of two spicules: the impact of spicules on the magnetic chromosphere // Publications of the Astronomical Society of Japan. 2007. V. 59. Iss. sp3. P. S655-S652. DOI: 10.1093/pasj/59.sp3.S655.

8. *Pereira T.M.D., De Pontieu B., Carlsson M.* Quantifying spicules // The Astrophysical J. 2012. V. 759. Iss. 1. Art.ID 18. DOI: 10.1088/0004-637X/759/1/18.

9. *Raouafi N.E., Patsourakos S., Pariat E. et al.* Solar coronal jets: observations, theory, and modeling //Space Science Reviews. 2016. V. 201. Art.ID 1-53. DOI: 10.1007/s11214-016-0260-5.

10. *Moore R. L., Cirtain J.W., Sterling A.C. et al.* Dichotomy of solar coronal jets: standard jets and blowout jets // The Astrophysical J. 2010. V. 720. Iss. 1. Art.ID 757. DOI: 10.1088/0004-637X/720/1/757.

11. *Moore R.L., Sterling A.C., Falconer D.A. et al.* The cool component and the dichotomy, lateral expansion, and axial rotation of solar X-ray jets // The Astrophysical J. 2013. V. 769. Iss. 2. Art.ID 134. DOI: 10.1088/0004-637X/769/2/134.

12. *Bohlin J.D., Vogel S.N., Purcell J.D. et al.* A newly observed solar feature-Macrospicules in He II 304 A // Astrophysical J. 1975. V. 197. Pt. 2. P. L133–L135. DOI: 10.1086/181794.

13. *Pereira T.M.D., De Pontieu B., Carlsson M. et al* . An interface region imaging spectrograph first view on solar spicules // The Astrophysical J. Letters. 2014. V. 792. Iss. 1. Art.ID L15. DOI: 10.1088/2041-8205/792/1/L15.

14. *Loboda I.P., Bogachev S.A.* What is a Macrospicule? // Astrophys. J. 2019. V. 871. Iss. 2. Art.ID 230. DOI: 10.3847/1538-4357/aafa7a.

15. *Loboda I.P., Bogachev S.A.* A statistical study of linear jets in the low solar corona // Astronomical and Astrophysical Transactions. 2019. V. 31. Iss. 2. P. 199–208.

16. *Bennett S.M., Erdélyi R.* On the statistics of macrospicules // The Astrophysical J. 2015. V. 808. Iss. 2. Art.ID 135. DOI: 10.1088/0004-637X/808/2/135.

17. *Kiss T.S., Gyenge N., Erdélyi R.* Systematic variations of macrospicule properties observed by SDO/AIA over half a decade // The Astrophysical J. 2017. V. 835. Iss. 1. Art.ID 47. DOI: 10.3847/1538-4357/aa5272.

18. *Lemen J.R., Title A.M., Akin D.J. et al.* The atmospheric imaging assembly (AIA) on the solar dynamics observatory (SDO) // Solar Physics. 2012. V. 275. P. 17–40. DOI: 10.1007/s11207-011-9776-8.

19. *Loboda I., Reva A., Bogachev S. et al.* Separating He II and Si XI Emission Components in Off-limb 304 Å Observations // Solar Physics. 2023. V. 298. Iss. 11. Art.ID 136. DOI: 10.1007/s11207-023-02230-6.

20. *Boerner P.F., Testa P., Warren H. et al.* Photometric and thermal cross-calibration of solar EUV instruments // Solar Physics. 2014. V. 289. P. 2377–2397. DOI: 10.1007/s11207-013-0452-z.

21. *Bogachev S.A., Loboda I.P., Reva A.A. et al.* Difference in the Characteristics of Solar Macrospicules at Low and High Latitudes // Astron. Lett. 2022. V. 48. Iss. 1. P. 47–54. DOI: 10.1134/S1063773722010029.

22. *Loboda I.P., Bogachev S.A.* Quiescent and eruptive prominences at solar minimum: a statistical study via an automated tracking system // Sol. Phys. 2015. V. 29. DOI: 10.1007/s11207-015-0735-7.

Figure Captions

Fig. 1. Distinction between main types of solar jets by rise height and lifetime.

Fig. 2. Example of observations of an eruptive jet formed by a minifilament eruption in 304 Å (a), 171 Å (b), and 193 Å (c) *SDO/AIA* channels. In the 171 and 193 Å channels (b, c), the movement of cold minifilament material is visible at the initial stage of the jet's motion, while the 193 Å channel (c) simultaneously shows the ejection of hot coronal material.

Fig. 3. Distribution of the main measured characteristics of solar jets in the EUV range. Separate data is shown for jets registered in quiet sun regions and coronal holes (a, b), linear and spiral jets (c-g), and jets with noticeable absorption or emission in 171 and 193 Å channels (h-k).

Fig. 4. The strongest correlations of measured jet characteristics. The color indicates the year of observation. Dashed lines show linear approximations along with the corresponding correlation coefficient values.

Fig. 5. Interdependence of lifetime and scale, expressed as average gravitational energy, for prominences and eruptive jets (a), as well as for different groups of jets (b). Dashed lines show linear approximations: red — for eruptive jets, black — for prominences (a) and all types of EUV jets (b).

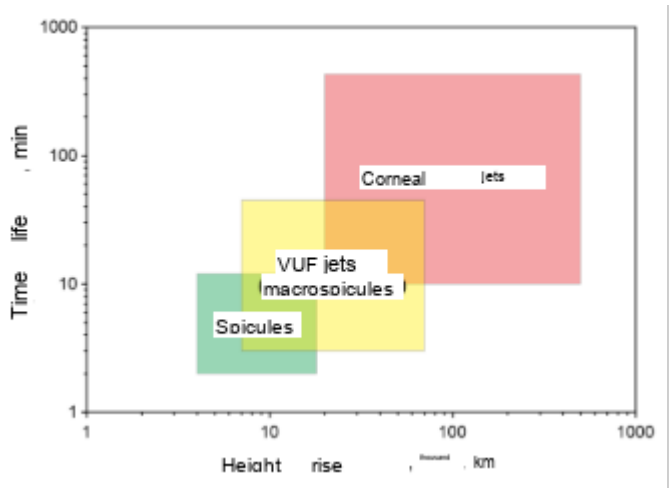

Fig. 1.

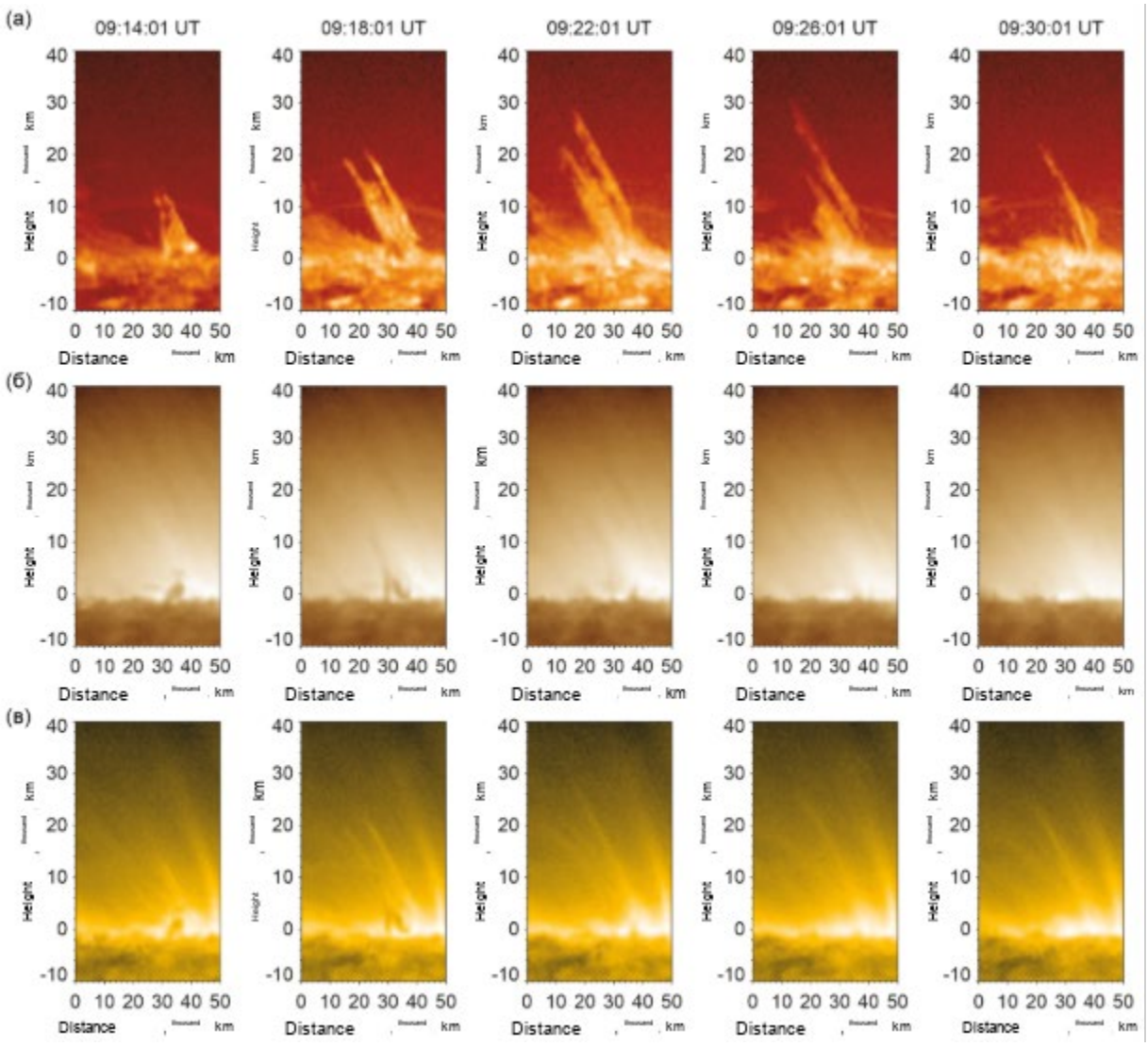
(а)
09:14:01 UT
09:18:01 UT
09:22:01 UT
09:26:01 UT
09:30:01 UT
(б)
(в)
Height, km
Distance, km
40
30
20
10
0
-10
0 10 20 30 40 50

Fig. 2.

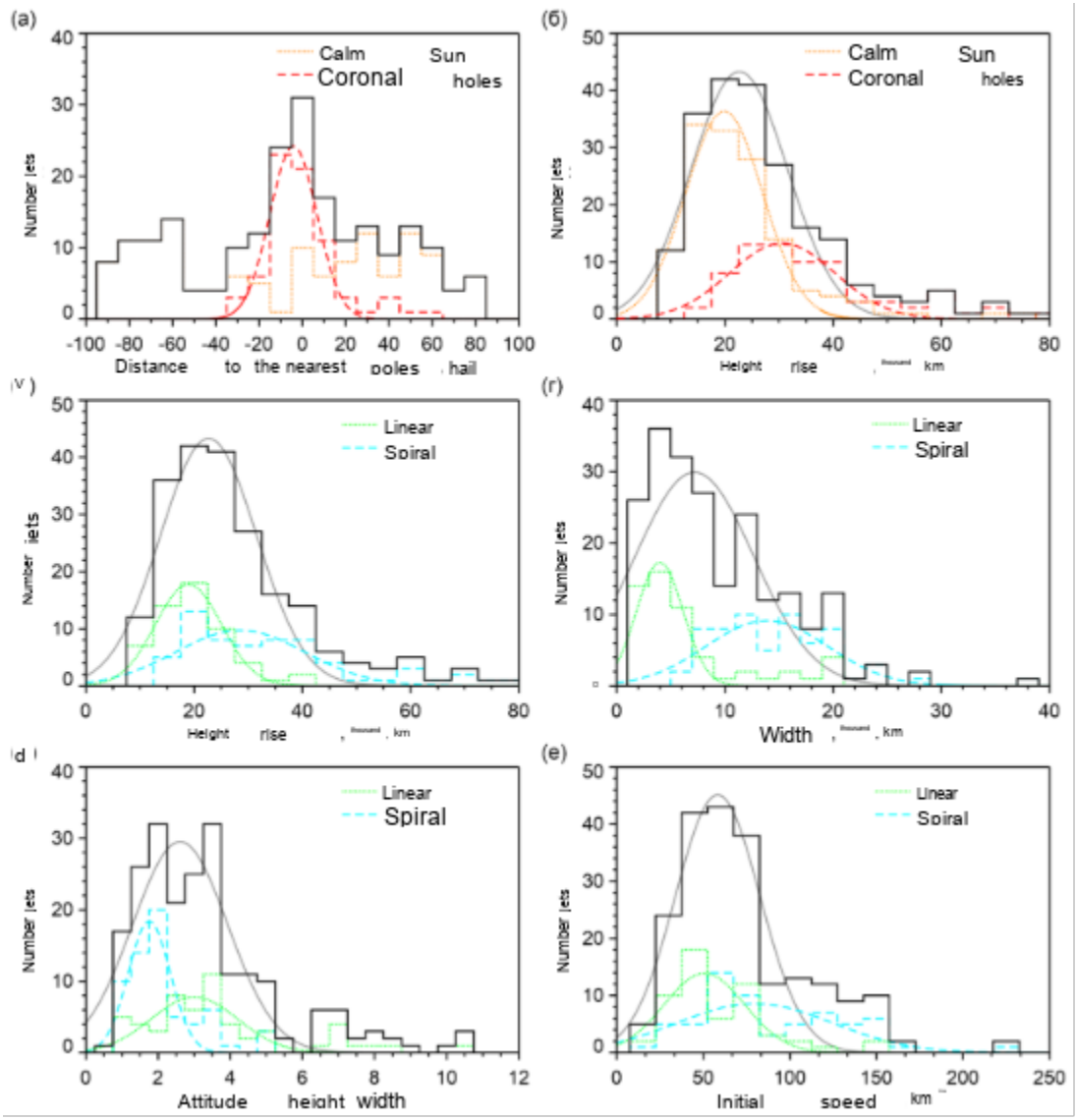
(a)
Calm
Coronal
Sun holes
Number jets
Distance to the nearest poles hail
(б)
Calm
Coronal
Sun holes
Number jets
Height rise km
(v)
Linear
Spiral
Number jets
Height rise km
(r)
Linear
Spiral
Number jets
Width km
(d)
Linear
Spiral
Number jets
Attitude height width
(e)
Linear
Spiral
Number jets
Initial speed km

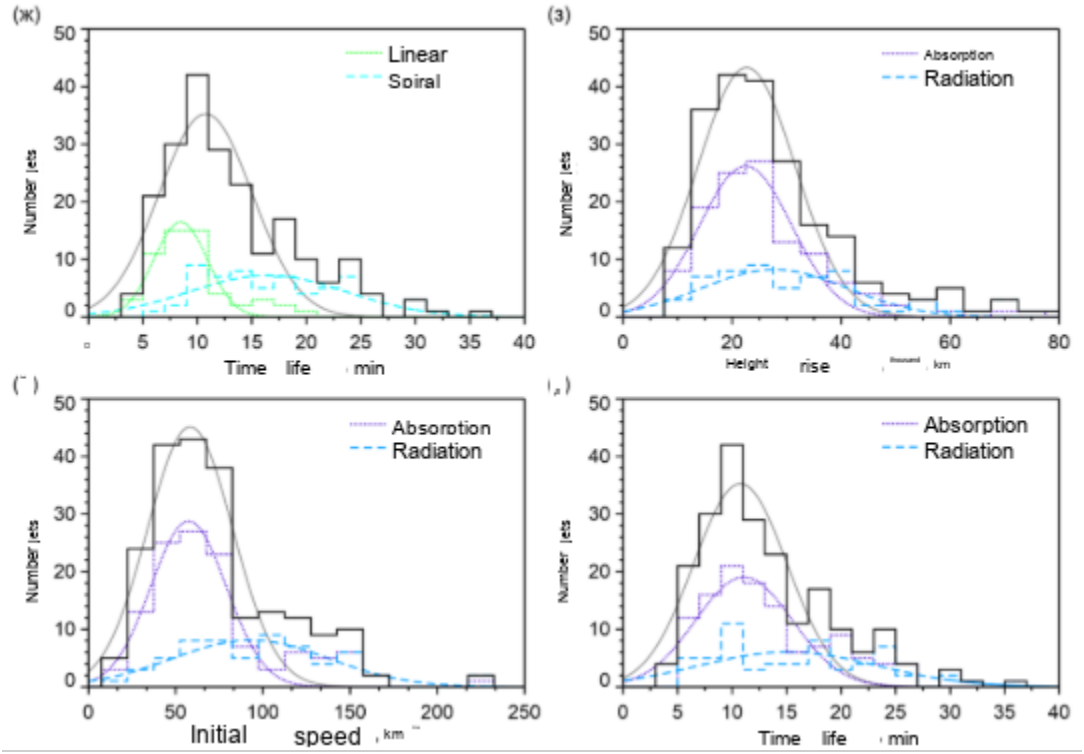

Fig. 3.

Fig. 3 (continued)

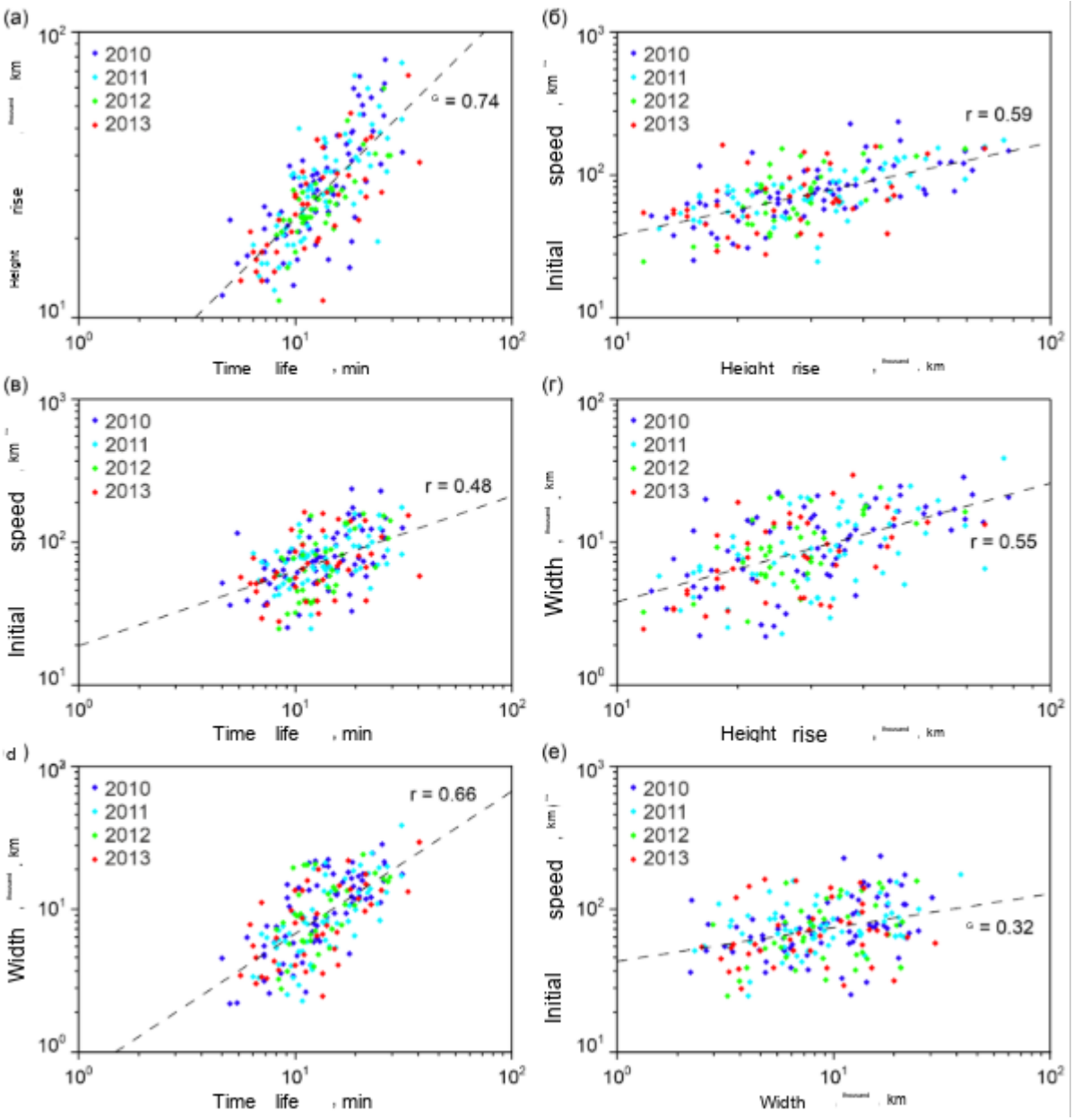
(а)
2010
2011
2012
2013
r = 0.74
Time life, min
(б)
r = 0.59
(в)
r = 0.48
(г)
r = 0.55
Height rise, km
(д)
r = 0.66
(е)
r = 0.32
Width, km

Fig. 4.

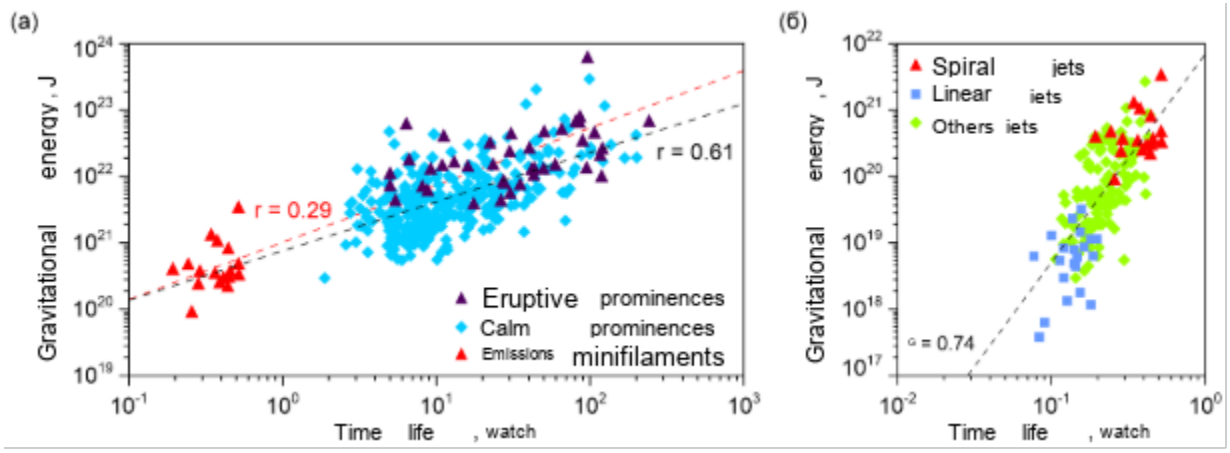
(a)
Gravitational energy, J
Time life, watch
r = 0.29
r = 0.61
Eruptive prominences
Calm prominences
Emissions minifilaments
(б)
Gravitational energy, J
Time life, watch
Spiral jets
Linear jets
Others jets
= 0.74

Fig. 5.